Dyes and Pigments 87 (2010) 149–157

Contents lists available at ScienceDirect

Dyes and Pigments

journal homepage: www.elsevier.com/locate/dyepig

The tautomerism, solvatochromism and non-linear optical properties of fluorescent 3-hydroxyquinoxaline-2-carboxalidine-4-aminoantipyrine

V. Arun [a], S. Mathew [b,c], P.P. Robinson [a], M. Jose [a], V.P.N. Nampoori [b,c], K.K.M. Yusuff [a,*]

[a] Department of Applied Chemistry, Cochin University of Science and Technology, Cochin 682 022, Kerala, India
[b] International School of Photonics, Cochin University of Science and Technology, Cochin 682 022, Kerala, India
[c] Centre of Excellence in Lasers and Optoelectronic Sciences, Cochin University of Science and Technology, Cochin 682 022, Kerala, India

ARTICLE INFO

Article history:
Received 2 January 2010
Received in revised form
10 March 2010
Accepted 11 March 2010
Available online 20 March 2010

Keywords:
Schiff base
Quinoxalines
Tautomerism
Fluorescence
Solvatochromism
Non-linear optical behaviour

ABSTRACT

The Schiff base, 3-hydroxyquinoxaline-2-carboxalidine-4-aminoantipyrine, was synthesized by the condensation of 3-hydroxyquinoxaline-2-carboxaldehyde with 4-aminoantipyrine. HPLC, FT-IR and NMR spectral data revealed that the compound exists predominantly in the amide tautomeric form and exhibits both absorption and fluorescence solvatochromism, large stokes shift, two electron quasi-reversible redox behaviour and good thermal stability, with a glass transition temperature of 104 °C. The third-order non-linear optical character was studied using open aperture Z-scan methodology employing 7 ns pulses at 532 nm. The third-order non-linear absorption coefficient, β, was 1.48×10^{-6} cm W^{-1} and the imaginary part of the third-order non-linear optical susceptibility, Im $\chi^{(3)}$, was 3.36×10^{-10} esu. The optical limiting threshold for the compound was found to be 340 MW cm^{-2}.

1. Introduction

Materials with excellent optical non-linearity and spectral characteristics are required for high-level technologies such as data storage, information processing, telecommunications and optical switching. Organic materials having π-extended frameworks with alternating single (σ) and double/triple bonds exhibit photoluminescence and enjoy many applications as organic light-emitting diodes (OLEDs) [1]. Fluorescent heterocyclic dyes whose fluorescence emission occurs at red wavelengths are expected to play a leading role in full color electroluminescence displays [2–7]. Several quinoxaline derivatives as well as heterocycles that contain a quinoxaline moiety have π-extended frameworks and are much used as photoluminesent molecules [8–10] and electron-transport materials in multilayer OLEDs [11,12]. For use in LEDs, a knowledge of the photophysical characteristics of the charge-transporting materials is of fundamental importance in terms of the optimisation of device properties and is also valuable for the design of potential new blue-light emitters [13]. In recent years, numerous reports on the photophysical properties of quinoxalines have appeared [14–23]. Organic compounds are also important for photonic devices because of their optical non-linear properties [24]. This paper concerns an investigation of the solvatochromism, tautomerism, electrochemistry, thermal analysis and non-linear optical character of the Schiff base, 3-hydroxyquinoxaline-2-carboxalidine-4-aminoantipyrine (HQCAAP).

2. Experimental

2.1. Materials

All chemicals were obtained from Sigma–Aldrich (Bangalore, India) and were used as supplied. Organic solvents used were purified and dried using standard methods.

2.2. Methods

Microanalyses of the compound was carried out using an Elementar Vario EL III CHNS elemental analyzer. Room-temperature FT-IR spectrum was recorded as KBr pellets using a JASCO FTIR 4100 Spectrophotometer in the 4000–400 cm^{-1} range. The electronic spectra of the Schiff base (10^{-5} mol l^{-1}) in different solvents were recorded on a Thermo Electron Nicolet Evolution 300 UV–VIS Spectrophotometer. The UV–Vis diffuse reflectance spectrum was recorded on a Labomed UV–Vis spectrophotometer equipped with

* Corresponding author. Tel./fax: +91 484 2575804.
E-mail addresses: yusuff@cusat.ac.in, yusuff15@gmail.com (K.K.M. Yusuff).

0143-7208/$ – see front matter © 2010 Elsevier Ltd. All rights reserved.
doi:10.1016/j.dyepig.2010.03.012

a diffuse reflectance accessory in the range 200–900 nm; %*R* values were converted to absorbance using the Kubelka Munk function. ^{1}H NMR and ^{13}C NMR spectra of the synthesized compound were recorded in DMSO-d_6 on a Bruker Avance DRX 500 MHZ NMR spectrometer. The fluorescence spectra of the compound (10^{-5} mol l^{-1}) in different solvents were recorded on a Cary Eclipse Fluorescence Spectrophotometer (Varian). The linear refractive index of the compound in ethanol was determined using a Sipcon Abbe Refractometer. TG–DTA–DTG analysis was carried out under a nitrogen atmosphere employing two different heating rates (10 °C min^{-1} and 20 °C min^{-1}) using a Perkin Elmer Pyres Diamond TG/DTA analyser. DSC analysis was carried out using a Mettler Toledo DSC 822e at a heating rate of 10 °C min^{-1} under nitrogen atmosphere. The powder X-ray diffraction pattern of HQCAAP was recorded on a Bruker model D8 (CuKα source) X-ray diffractometer form 2-theta values 5–120° at a step time 0.2 s. Cyclic voltammetric studies were carried out with a BAS EPSILON Electrochemical Analyser using glassy-carbon working electrode. A Pt wire and Ag/AgCl were used as counter and reference electrodes, respectively.

HPLC analysis was performed using a Dionex UltiMate 3000 HPLC system equipped with pump, autosampler column compartment, photodiode array detector and Chromeleon software. Separation was carried out using an Acclaim 120 column, C18 5 μm 120 Å (4.6 × 250 mm), with a guard column packed with the same material. The column was maintained at 30 °C throughout the analysis and detection was carried out at 254 nm. HPLC grade acetonitrile and water (Qualigens) were used for sample preparation and as mobile phase; the mobile phase used was 70% acetonitrile–water with a flow rate of 1 mL/min.

The third-order non-linear optical character was determined using the single beam, Z-scan technique employing a 1.0 × 10^{-5} mol L^{-1} ethanolic solution of the compound. A Q-switched Nd:YAG laser (Spectra Physics LAB-1760, 532 nm, 7 ns, 10 Hz) was used as light source. The sample was moved in the direction of light at the focal point of the lens (focal length 200 mm), the radius of the beam waist being calculated as 35.467 μm. The Rayleigh length, Z_R was estimated to be 7.42 mm, this being much greater than the thickness of the sample cuvette (1.1 mm), which is an essential prerequisite for Z-scan experiments. The transmitted beam energy, reference beam energy and their ratio were measured simultaneously using an energy ratiometer (Rj7620, Laser Probe Corp.) having two identical pyroelectric detector heads (Rjp735). The effect of fluctuations of laser power was eliminated by dividing the transmitted power by the power obtained at the reference detector; both measured using identical photo detectors. The schematic diagram of the experimental setup used is shown in Fig. 1.

2.3. Synthesis of HQCAAP

The Schiff base, 3-hydroxyquinoxaline-2-carboxalidine-4-aminoantipyrine (HQCAAP), was synthesized by employing the procedure of Arun et al. [25]. Yield: (90%, 9.3 g). Anal. Cald. for $C_{20}H_{17}N_5O_2$ (359.38): C, 66.84; H, 4.77; N, 19.47. Found: C, 66.68; H, 4.65; N, 19.32. IR (cm^{-1}): 3451, 3038, 3009, 2928, 2901, 2837, 2712, 1670, 1656, 1637, 1591, 1551, 1489, 1455, 1414, 1384, 1350, 1306, 1268, 1224, 1154, 1134, 1069, 1045, 1023, 949, 856, 817, 771, 757, 703, 685, 625, 592, 575, 543, 513, 488, 468, 412. λ_{max}(nm) in methanol (10^{-5} mol l^{-1}) = 210, 224, 423; ε_{max} (L mol^{-1} cm^{-1}) = 1.98 × 10^5, 1.90 × 10^5, 1.45 × 10^5. ^{1}H NMR δ ppm: (500 MHz, DMSO-d_6, 296 K): δ = 2.49 (s, 3H, C–CH$_3$), 3.27 (s, 3H, N–CH$_3$), 7.28–7.85 (9H, Ar–H), 9.98 (s, 1H, azomethine proton), 12.51 (s, 1H, Ar–OH or N–H).

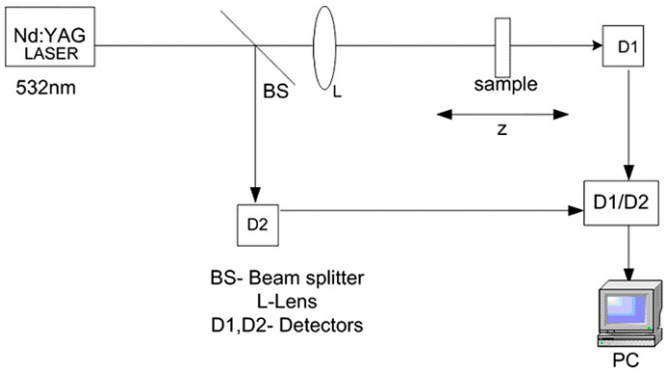

Fig. 1. Schematic diagram of the experimental setup for the Z-scan measurement.

3. Results and discussion

Hydroxyquinoxalines and their derivatives exhibit prototropic amide–iminol tautomerism and most of them exist in the predominant amide form in the solid state [23,25–30]. Crystalline nature of the HQCAAP is confirmed from the presence of well defined peaks in its powder XRD pattern (Fig. 2). The IR spectrum of the HQCAAP shows one broad, strong absorption band at 3451 cm^{-1} which is either due to a hydrogen bonded $\nu_{(OH)}$ in the iminol tautomer or $\nu_{(NH)}$ in the amide tautomer. In the amide tautomeric form, the molecule contains two types of ketonic groups, one attached to the quinoxaline ring and the other in the pyrazoline ring. The pyrazoline carbonyl stretch in the case of Schiff base ligands derived from 4-aminoantipyrine and substituted salicylaldehydes is in the 1616–1665 cm^{-1} range [31]. In the present case, there is a strong band at 1656 cm^{-1} which may be due to the $\nu_{C=O}$ stretch of the pyrazoline ring of the Schiff base. The peaks observed at 1670 cm^{-1} may be due to the C=O group of the amide tautomer of the Schiff base. Although HQCAAP contains three different types of C=N bonds, two from the quinoxaline ring and one from the azomethine linkage, they are not well resolved in the infrared spectrum. The azomethine –CH=N band is superimposed with the C=O group of the amide tautomer and appear as a weak band at 1637 cm^{-1}. The $\nu_{(C=N)}$ stretch of the quinoxaline ring is observed at 1591 cm^{-1} [25]. The $\nu_{(C=N)}$ (azomenthine) falls in between $\nu_{(C=O)}$ group of the amide tautomer and the $\nu_{(C=N)}$ of the quinoxaline ring.

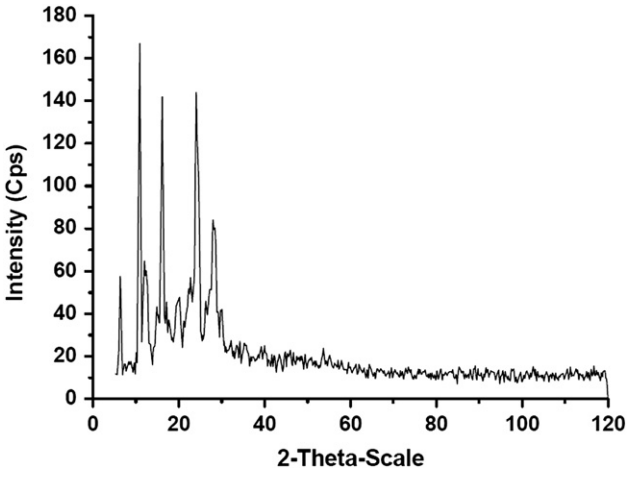

Fig. 2. Powder XRD pattern of HQCAAP.

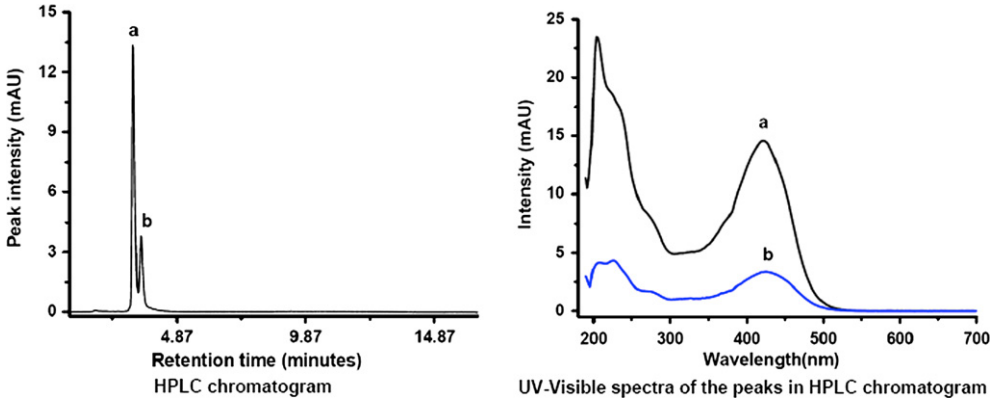

Fig. 3. HPLC chromatogram of HQCAAP in acetonitrile and UV–visible spectra of the peaks.

The ^{1}H NMR spectrum of the HQCAAP shows singlet peaks at δ 3.27 ppm and δ 2.49 ppm due to the N–CH_3 and C–CH_3 groups of the pyrazolone ring respectively. The multiplet in the range δ 7.85 to 7.28 ppm is due to the different aromatic protons of the 3-hydroxyquinoxaline-2-carbaxalidine-4-aminoantipyrine. The singlet peak at δ 9.98 ppm is due to the azomethine proton of the Schiff base. The peaks at δ 12.54 ppm and δ 12.51 ppm are assignable to the proton of the N–H of the amide tautomer or O–H of the iminol form of the Schiff base [23].

The HPLC analysis of the HQCAAP in acetonitrile (10^{-4} mol l^{-1}) reveals that the compound may exist in two forms. The HPLC chromatogram (Fig. 3) gave two peaks: one with retention time 3.18 min (a) having relative area percentage of 72.3 and another with 3.48 min (b) having the relative area percentage of 27.7 indicating the existence of the compound in two forms. For the peak, *a*, the absorption occurs at 203, 234 (shoulder), 275 (shoulder), and 422 nm and for *b*, it occurs at 206, 225, 275 (shoulder) and 424 nm. The electronic spectrum of the species corresponding to the major peak is due to the amide form and that corresponding to the minor peak is due to the iminol from [23]. Thus the Schiff base exhibits prototropic tautomerism and exists in the predominant amide form. The two tautomeric structures are shown in the Scheme 1.

To study the effect of solvent on the absorption spectrum, we recorded the spectrum of HQCAAP in solid state and in various solvents with different polarities. The concentration of the solution was 10^{-5} mol l^{-1}. The solvents used were methanol, ethanol, isopropyl alcohol, tetrahydrofuran, acetonitrile, dichloromethane, dimethylformamide, dimethyl sulphoxide, ethylacetate, equimolar HQCAAP and NaOH in methanol and 1:1 hexane–methanol. The solid state diffuse reflectance spectrum (DRS) of HQCAAP shows bands at 253 nm, 354 nm, 482 nm and 625 nm (shoulder). The first one is due to the $\pi \rightarrow \pi^*$ transitions of the heterocyclic quinoxaline ring and the second one is due to the $n \rightarrow \pi^*$ transition of the –C=N– group in quinoxaline ring [23]. The azomethine $n \rightarrow \pi^*$ transition appears at 482 nm. The shoulder band at 625 nm may be due to the intramolecular charge transfer transition. The highest energy absorption bands in the solution spectra (all solvents) are assigned to $\pi \rightarrow \pi^*$ transitions by virtue of their large molar extinction coefficients (Table 1). The $n \rightarrow \pi^*$ transitions of the quinoxaline ring appears as a shoulder band around 355 nm [23]. The band centered on 420 nm is due to the $n \rightarrow \pi^*$ transitions of the azomethine group.

The absorption peaks are blue shifted in solution with respect to the peaks in the DRS spectrum. In solution, the ground state of HQCAAP is stabilized by hydrogen bonding with the solvent. In the excited state, the hydrogen bond of the molecule is almost completely broken or weakened to a larger extend. As a result the excited state is less stabilized and absorption is shifted to higher energy [32,33].

The longest wave length absorption band of HQCAAP in various solvents lies between 415 and 431 nm and is seen to increase with increasing solvent polarity (Fig. 4). This positive solvatochromism exhibited by the compound may be due to the effect of dipole moment changes of the excited state, changes in the hydrogen bonding strength and/or due to excited state protonation [32,33]. Furthermore, in the present case there is a possibility for the polarization of the lactam system of the pyrazolone ring leading to a net negative charge on the oxygen atom [34], which may also influence the absorption characteristics of HQCAAP. To study the absorption characteristic of the enolate anion of HQCAAP, we recorded the UV–Vis spectrum in methanol containing an equivalent amount of NaOH (Table 1). The enolate anion, formed by the dissolution of HQCAAP in an equivalent amount of NaOH in

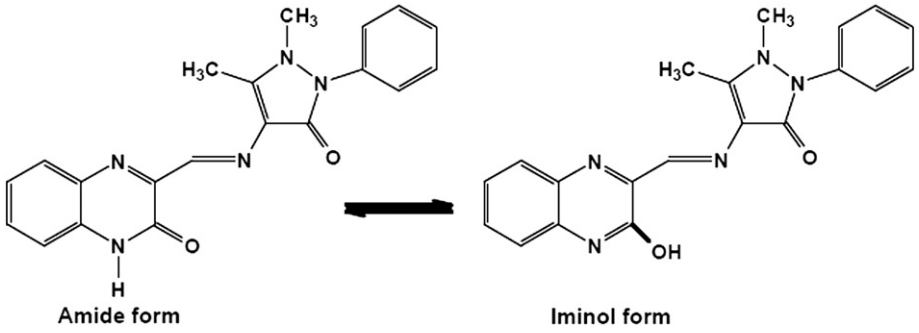

Scheme 1. Amide–iminol tautomerism in HQCAAP.

Table 1
Absorption spectral data of HQCAAP.

Solvent	λ_{max}(nm) ($\varepsilon_{max} \times 10^{-5}$ (L mol^{-1} cm^{-1}))
Ethanol	204 (1.09); 231 (0.55)^{sh}; 425 (0.26)
Methanol	210 (1.98); 224 (1.90); 275 (0.77)^{sh}; 325 (0.51)^{sh}; 422 (1.45)
IPA	213 (1.92); 253 (0.30); 262 (0.29); 269 (0.26); 422 (0.25)
Ethylacetate	252 (0.26); 268 (0.21); 415 (0.36)
Acetonitrile	205 (2.02); 231 (0.79)^{sh}; 420 (0.71)
THF	242 (0.50); 294 (0.25); 415 (0.40)
DCM	228 (0.48); 284 (0.21)^{sh}; 316 (0.17)^{sh}; 410 (0.28); 501 (0.07)^{sh}
DMF	268 (0.32); 427 (0.41)
Acetic acid	342 (1.16); 413 (0.15)^{sh}
X1	193 (0.54); 203 (0.54); 223 (0.47); 225 (0.46); 432 (0.31)
DRS	253, 354, 415^{sh}, 482, 625^{sh}

IPA = isopropyl alcohol; THF = tetrahydrofuran; DCM = dichloromethane; DMF = dimethylformamide; DMSO = dimethyl sulphoxide; X1 = equimolar HQCAAP and NaOH in methanol; DRS = diffuse reflectance spectrum; sh = shoulder peak.

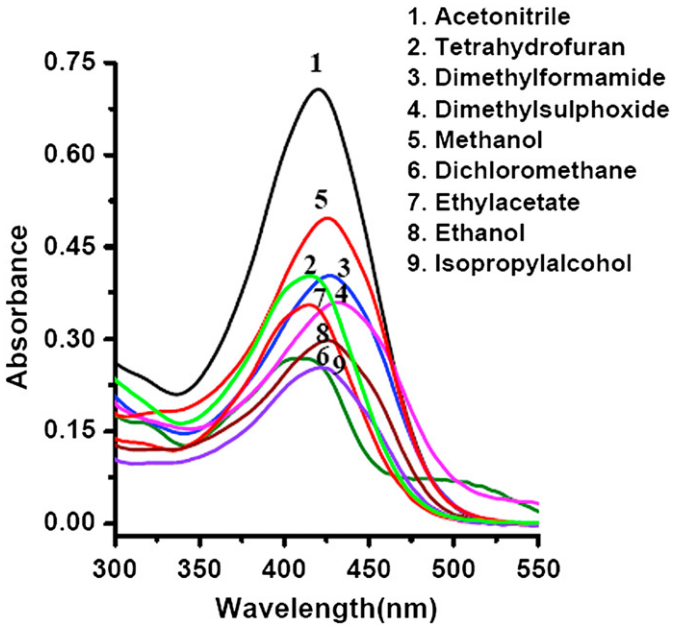

Fig. 4. Longest wave length absorption bands of HQCAAP in various solvents.

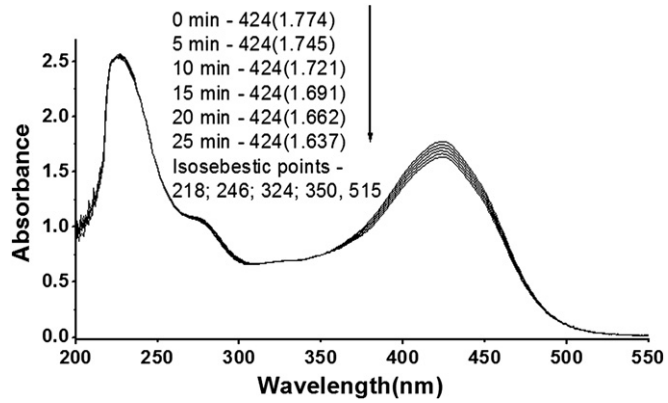

Fig. 5. The UV–Vis spectra of HQCAAP in 1:1 methanol–hexane mixture at different time intervals.

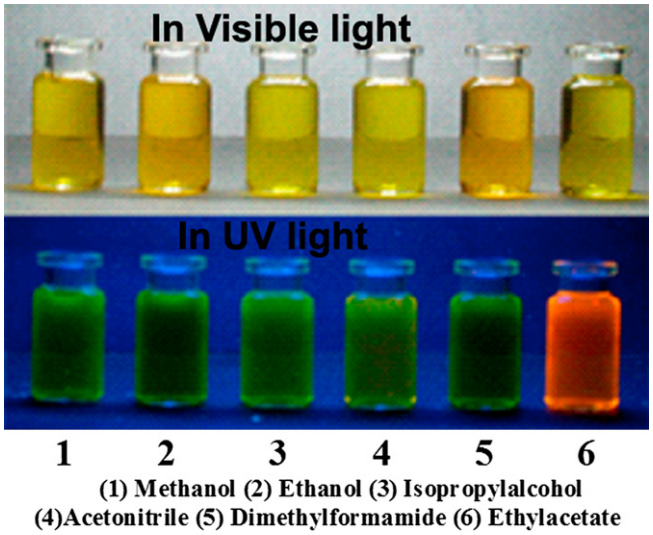

Fig. 6. Different colours exhibited by HQCAAP in visible and UV light (For interpretation of the references to colour in this figure legend, the reader is referred to the web version of this article).

methanol, absorbs at a higher wavelength compared to the non-enolate from [35,36]. Also the presence of well defined isosebestic points (at 218, 246 324, 350 and 515 nm) in the UV–Vis spectra of HQCAAP recorded in 1:1 methanol–hexane mixtures (10^{-5} mol l^{-1}) at different time intervals (Fig. 5) reveal that in this medium the compound contains more than one absorbing species [37].

The compound, HQCAAP, shows different colours in UV light and this prompted us to study its fluorescent behaviour. A comparison of the different colours exhibited by the compound in visible and UV light is shown in Fig. 6. The photoluminescence spectra of the compound in various solvents (10^{-5} mol L^{-1}) at two different excitation wavelength (270 and 430 nm) were recorded and are not identical. At the excitation wavelength 430 nm

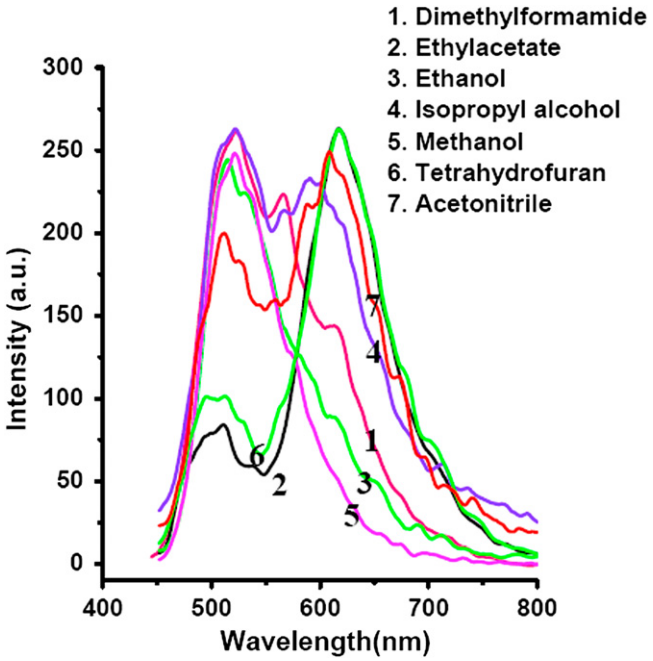

Fig. 7. Photoluminescence spectra of HQCAAP in various solvents at the excitation wavelength 430 nm.

Table 2
Fluorescence spectral data and Stokes shift of HQCAAP in various solvents.

Solvent	$F^{\#}$ (nm)	F^{*} (nm)	A (nm)	$S^{\#}$ (nm)	S^{*} (nm)
Ethanol	515	308, 526	425	90	101
Methanol	521	368, 503	423	98	80
IPA	520, 593	307, 512, 593	422	171	171
Ethylacetate	510, 617	312, 493, 622	415	202	207
Acetonitrile	511, 609	502, 616	420	189	196
THF	512, 618	310, 485, 615	415	203	200
DMF	525, 567	353, 517, 569, 614	427	140	187

IPA = isopropyl alcohol; THF = tetrahydrofuran; DMF = dimethylformamide; A = longest wavelength of absorption; F = flourescence; S = Stokes shift; # = excitation at 430 nm; * = excitation at 270 nm.

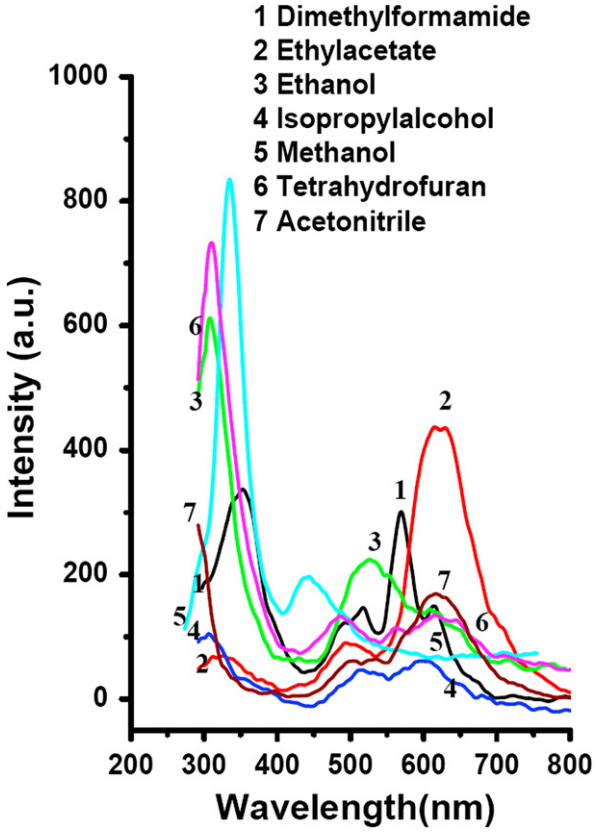

Fig. 8. Photoluminescence spectra of HQCAAP in various solvents at the excitation wavelength 270 nm.

Table 3
Electrochemical data of HQCAAP in acetonitrile.

Scan rate (mV)	(E_{pc}, mV)	(E_{pa}, mV)	(I_{pc}, μV)	(I_{pa}, μV)	(I_{pc}/I_{pa})
20	−825	−693	9.40	4.63	2.03
40	−850	−690	19.66	9.35	2.10
60	−856	−686	24.70	11.35	2.18
80	−865	−676	28.85	13.33	2.16
100	−871	−671	32.08	14.75	2.17
150	−880	−671	41.18	18.88	2.18

E_{pc} = cathodic peak potential; E_{pa} = anodic peak potential; I_{pc} = cathodic peak current; I_{pa} = anodic peak current; I_{pc}/I_{pa} = number of electrons.

HQCAAP exhibits a single emission peak in methanol and ethanol and dual fluorescence with two well resolved fluorescence bands in all other solvents (Fig. 7 and Table 2). However the compound exhibits dual fluorescence in all solvents at the excitation wavelength 270 nm (Fig. 8 and Table 2).

The emission maximum is shifted to shorter wavelength in more polar solvents, thus exhibiting a negative fluorescent solvatochromism, which indicates that the molecules become less polar in the excited states than in the ground state. The stokes shift in various solvents were seen to vary in the range 80–207 nm (Table 2). The large stokes shift for the present case may be either due to its less rigid structure or due to significant molecular rearrangement, that takes place upon photoexcitation. The stokes shift decreases with increasing solvent polarity.

Eventhough the HQCAAP is crystalline, it forms thin films, which is evident from its optical spectra of the acetone solution coated on a quartz plate by thermal evaporation technique. The UV–Visible absorption spectrum and photoluminascent spectrum with an excitation wavelength 430 nm of the thin film of the compound are shown in Fig. 9. This absorption spectrum of HQCAAP is characterized by three major absorption peaks at 214, 332 and 463 nm; where as, its photoluminascent spectrum with an excitation wavelength 430 nm exhibits duel emission at 483 and 530 nm.

To get more insight into the tautomeric structure of the compound, we recorded the cyclic voltammograms in less polar acetonitrile and comparatively more polar 1:1 THF–methanol mixtures with six different scan rates. Concentration of HQCAAP was 5×10^{-5} mol l^{-1} and the supporting electrolyte used was tetra *n*-butylammonium hexfluorophosphate (0.1 mol l^{-1}). The Schiff base, HQCAAP, exhibits different cyclic voltammetric behaviours in acetonitrile and 1:1 methanol–THF mixtures. The electrochemical data are given in Tables 3 and 4.

In acetonitrile all the curves have the same shape but different peak currents (Fig. 10). As the scan rate increases, the peak height is also increasing, however, the position of the peak current both for

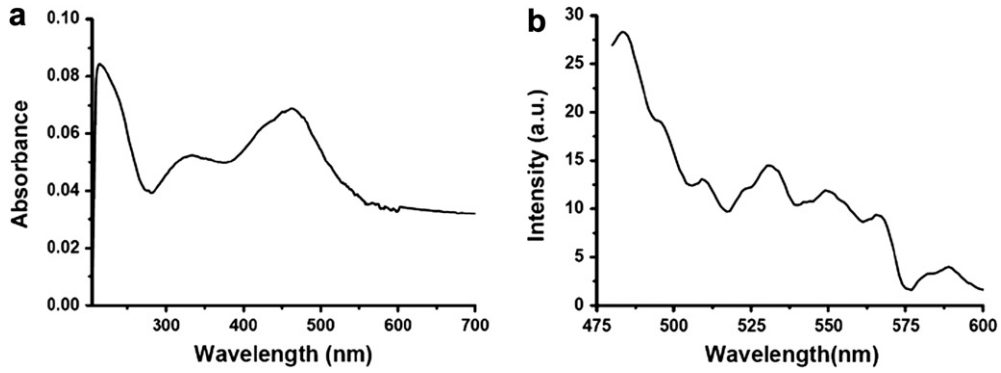

Fig. 9. The UV–Visible absorption spectrum (a) and photoluminascent spectrum with an excitation wavelength 430 nm (b) of the thin film of the HQCAAP.

Table 4
Electrochemical data of HQCAAP in 1:1 methanol–tetrahydrofuran.

Scan rate (mV)	(E_{pc}, mV)	(E_{pa}, mV)	(I_{pc}, μV)	(I_{pa}, μV)	(I_{pc}/I_{pa})
50	191	8, −995	5.04	4.23	1.19
100	104	96, −906	8.68	8.66	1.00
150	−7	224, −834	19.74	18.53	1.07
200	−73, −320	310, −790	30.65	29.91	1.02
250	−154, −387	352, −734	31.59	31.13	1.01
300	−198, −422	385, −711	42.25	39.37	1.07

E_{pc} = cathodic peak potential; E_{pa} = anodic peak potential; I_{pc} = cathodic peak current; I_{pa} = anodic peak current; I_{pc}/I_{pa} = number of electrons.

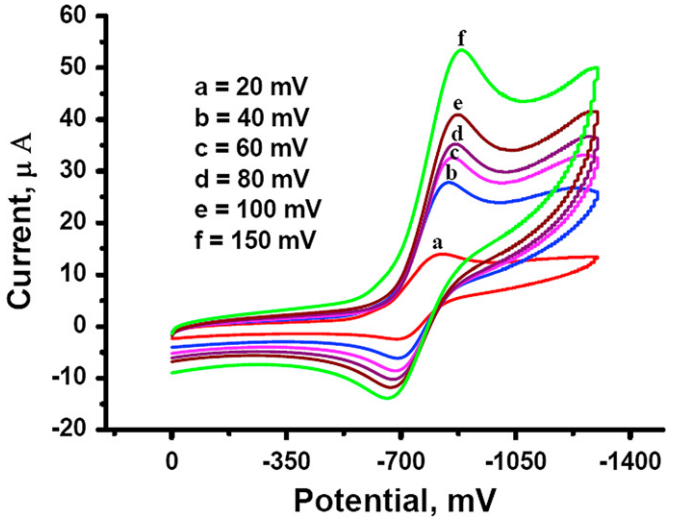

Fig. 10. Cyclic voltammograms of HQCAAP in acetonitrile.

the forward and reverse scan does not change. This is a characteristic of reversible electron transfer reaction [38]. For each scan the $I_{pc}/I_{pa} = 2.03$ which corresponds to two electron transfer during the redox process. In the less polar acetonitrile, the compound may be in the amide form and has a mobile proton in the N–H group of the quinoxaline fragment. During the oxidation step, the proton is possibly eliminated (Scheme 2). The positive charge, which arises in the product, facilitates the two electron oxidation. Similar observations were found for 3-indolysine-2-yl-quinoxalines [39].

The cyclic voltammetric behaviour of HQCAAP in 1:1 mixture of methanol–tetrahydrofuran (Fig. 11) is characterized by one reduction peak and two oxidation peaks and are strongly dependent upon the scan rate. As the scan rate is increased, a new cathodic peak is observed and its peak height increased with further increase in scan rate. This wave splitting might be due to a self protonation mechanism involving the proton transfer from the acidic iminol

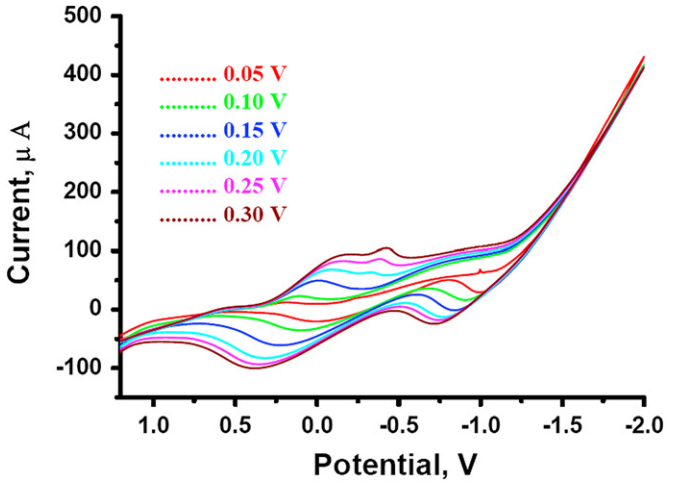

Fig. 11. Cyclic voltammograms of HQCAAP in 1:1 mixture of methanol–tetrahydrofuran.

form to basic reduction intermediate [40,41]. Hence in less polar acetonitrile, HQCAAP exhibits cyclic voltammograms characteristic of the amide tautomer, and in comparatively more polar methanol–tetrahydrofuran mixture it shows cyclic voltammograms characteristics of its iminol tautomeric from. Generally the fluorescent heteroaromatic compounds with imine nitrogen atoms (C=N) exhibiting less negative reduction potential compared to the analogous aromatic hydrocarbons and heteroaromatic rings with oxygen or sulphur atoms are reported as good candidates for n-type semiconductors in organic electronics [42]. HQCAAP exhibits half wave reduction potential at −0.77 V (in acetonitrile), which is comparatively more positive than that exhibited by pyrazine (−2.08 V) and quinoxaline (−1.62 V) [43] which indicates that it is a better choice for n-type organic semiconductor.

Thermal properties of HQCAAP were determined by TG–DTA–DTG and DSC measurements in the temperature range 40–600 °C. The DSC thermogram is shown in the Fig. 12 and TG–DTA–DTG curves for the HQCAAP under nitrogen atmosphere with two different heating rates (10 °C min^{-1} and 20 °C min^{-1}) are given in Fig. 13. In DTA, no sharp endothermic peak corresponding to melting was observed; instead of that one exothermic peak was observed at 245 °C, suggesting the compound to have no sharp melting. The compound may undergo some decomposition/phase change without melting. The first two exothermic peaks in DSC correspond to the loss of two water molecules which might be hydrogen bonded to the HQCAAP. One water molecule may be hydrogen bonded with the oxygen of the pyrazolone ring and the other may be hydrogen bonded with the amide N–H of the quinoxaline ring. However, in the TG curves, the mass loss

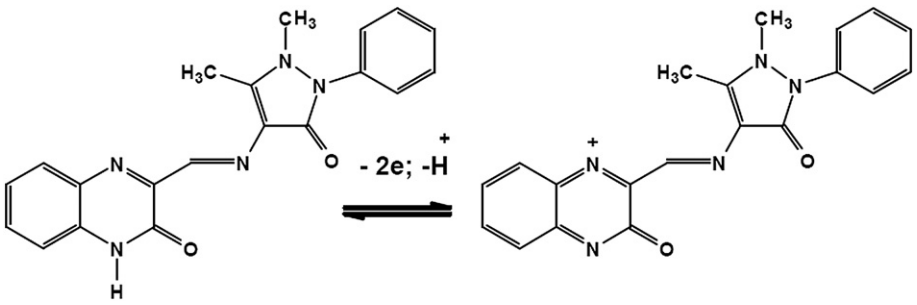

Scheme 2. Two electron transfer in HQCAAP.

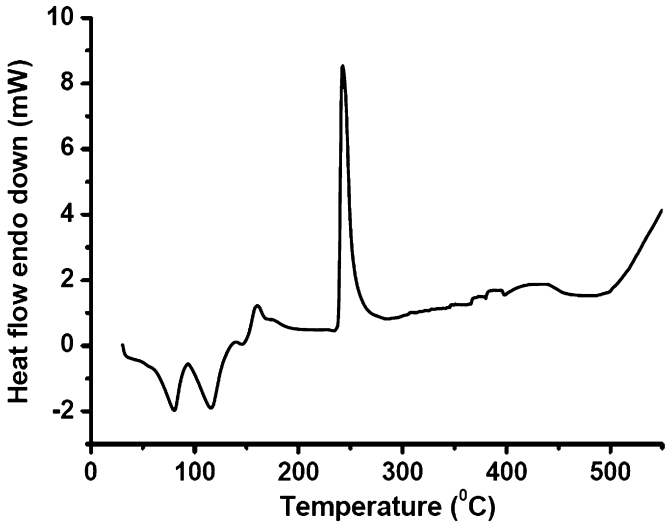

Fig. 12. DSC thermogram of HQCAAP.

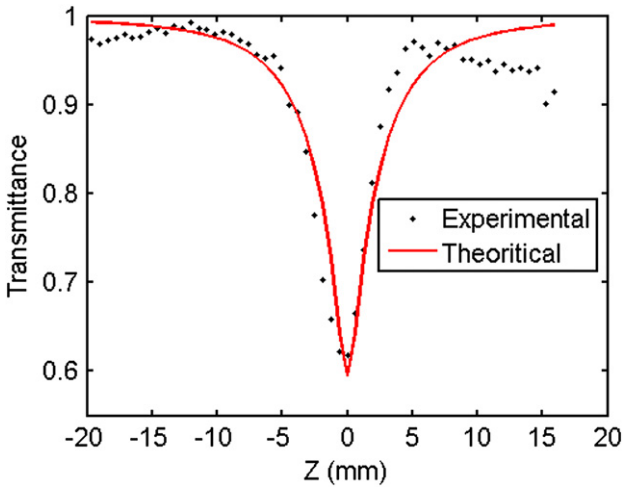

Fig. 14. Open aperture Z-scan curve for HQCAAP.

corresponding to removal of water of crystallization occurs in a single step below 110 °C (in the temperature range 45–100 °C for 10 °C min^{-1} and in the temperature range 50–110 °C for 20 °C min^{-1}). As the heating rate decreased form 20–10 °C min^{-1}, both the peaks corresponding to the loss of crystallized water molecules and the decomposition of the compound shifted to lower temperatures (Fig. 13). The procedure employed by Li et al. [44] was used to find out the glass transition temperature; T_g. For this, the compound was heated upto the 220 °C (below the decomposition temperature) and then was quickly cooled by swirling water. When the resulting amorphous glass of the compound was heated for the second time, a glass transition phenomenon was observed at 104 °C in the DSC. In principle, all the organic compounds for electroluminescent (EL) devices should have high T_g values [44]. Comparatively higher value for T_g (104 °C) suggests the application potential of this compound for EL devices.

In the present investigation, Z-scan technique developed by Sheik Bahae et al. [45] is used for measuring the non-linear absorption coefficient, imaginary part of the third-order non-linear susceptibility and optical limiting threshold of HQCAAP. The open aperture Z-scan curve for the HQCAAP is shown in Fig. 14 and the scatter dots are experimental data while the solid line is the theoretically fitted curve. The open aperture Z-scan curve shows a normalized transmittance valley, indicating the presence of reverse saturable absorption (RSA) in the compound. The obtained non-linearity is found to be of the third-order, as it fits to a two photon absorption process. The corresponding net transmission is given by,

$$T(z) = \frac{C}{q_0\sqrt{\pi}} \int_{-\infty}^{\infty} \ln(1+q_0 e^{-t^2})\mathrm{d}t \quad \text{where}$$

$$q_0(z,r,t) = \beta I_o(t) L_{\text{eff}} \tag{1}$$

Here, $L_{\text{eff}} = 1 - e^{-\alpha l}/\alpha$ is the effective thickness of the sample with linear absorption coefficient, α and thickness of the sample, l. β and I_o are the non-linear absorption coefficient and the irradiance at focus respectively.

The non-linear absorption coefficient, β, is obtained by fitting the experimental data to the equation (1). The constant, q_0 is obtained as the fit parameter and knowing the values of I_o and L_{eff}, the non-linear absorption coefficient can be calculated. The calculated value of non-linear absorption coefficient at an intensity of 0.795 GW/cm^2 (I_o) is 1.48 × 10^{-6} cm/W. The imaginary part of the third-order non-linear susceptibility can be calculated from non-linear absorption coefficient using the relation, $\mathrm{Im}(\chi^3) = n_0^2\lambda c\beta/480\pi^3$ in esu, where n_0 is the linear refractive index of the sample, HQCAAP, in ethanol (1.453), λ is the laser wavelength, c is the velocity of light in vacuum and its value obtained is 3.36 × 10^{-10} esu.

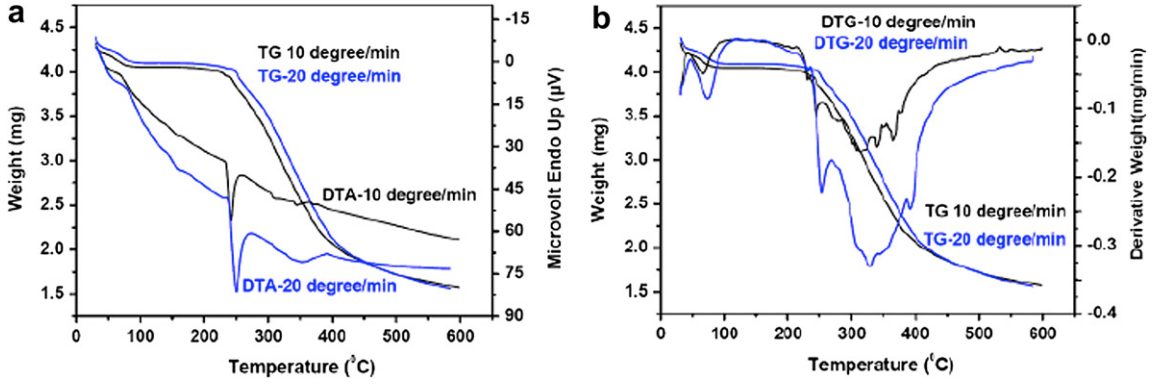

Fig. 13. TG–DTA–DTG curves for the HQCAAP under nitrogen atmosphere at 10 °C min^{-1} and 20 °C min^{-1}.

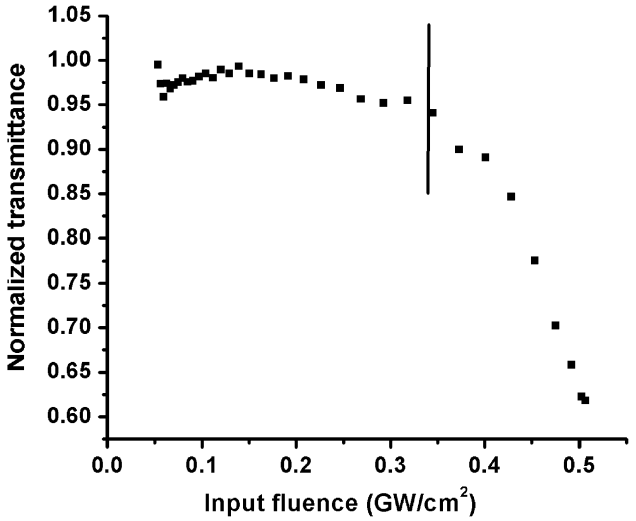

Fig. 15. Optical limiting response of the HQCAAP.

To study the optical limiting property of the sample, the non-linear transmission of the sample is studied as a function of input fluence. Optical power limiting is operated through the non-linear optical processes of the sample and an important term in the optical limiting measurement is the optical limiting threshold. The optical limiting property of the compound can be estimated from its Z-scan plots for various input fluences. For this, the non-linear transmission has to be plotted as a function of input fluences. From the value of fluence at focus, the fluence values at other positions could be calculated using the standard equations for Gaussian beam waist given by;

$$\omega^2(z) = \omega_0^2\left\{1 + \frac{z^2}{z_R^2}\right\} \quad (2)$$

Fig. 15 illustrates the optical limiting response of the sample. The vertical line in the figure indicates the approximate fluence at which the normalized transmission begins to deviate from its linearity which is considered as the optical limiting threshold value. The fluence value corresponding to the onset of optical limiting is found to be 340 MW/cm^2.

4. Conclusion

The Schiff base, HQCAAP, is polar and exhibts amide–iminol tautomerism. Its polarity decreases in solution. It exhibits positive solvatochromism in its absorption spectra where as a negative solvatochromism in its emission spectra in various solvents. The results of the UV–Vis, fluorescence, CV and DSC studies suggest that the present compound is a suitable candidate for application in organic electronics. The values of third-order non-linear absorption coefficient, β, imaginary part of the third-order non-linear optical susceptibility, Im $\chi^{(3)}$, and optical limiting threshold suggest that this compound might find application in the photonic age.

Acknowledgement

The authors thank Department of Science and Technology, India, for using the Sophisticated Analytical Instrumentation Facility (SAIF) at STIC, Cochin University of Science and Technology, Cochin for elemental analyses and DSC measurement. We also thank Dr. A. Ajayaghosh, NIIST, Trivandrum, Kerala for the ^{1}H NMR and ^{13}C NMR spectra.

References

[1] Shirota Y, Kageyama H. Charge carrier transporting molecular materials and their applications in devices. Chemical Reviews 2007;107(4):953–1010.
[2] Tang CW, VanSlyke SA, Chen CH. Electroluminescence of doped organic thin films. Journal of Applied Physics 1989;65(9):3610–6.
[3] Baldo MA, Lamansky S, Burrows PE, Thompson ME, Forrest SR. Very high-efficiency green organic light-emitting devices based on electrophosphorescence. Applied Physics Letters 1999;75(1):4–6.
[4] Chen C-T. Evolution of red organic light-emitting diodes: materials and devices. Chemistry of Materials 2004;16(23):4389–400.
[5] Huang Q, Evmenenko GA, Dutta P, Lee P, Armstrong NR, Marks TJ. Covalently bound hole-Injecting nanostructures. Systematics of molecular architecture, thickness, saturation, and electron-blocking characteristics on organic light-emitting diode luminance, turn-on voltage, and quantum efficiency. Journal of the American Chemical Society 2005;127(29):10227–42.
[6] Gondek E, Calus S, Danel A, Kityk AV. Photoluminescence and electroluminescence of methoxy and carboethoxy derivatives of 1,3-diphenyl-1-Hpyrazolo[3,4-b]quinoline. Spectrochimica Acta Part A: Molecular and Biomolecular Spectroscopy 2008;69(1):22–6.
[7] Yu S, Ma C, Cheng C, Wang X, Ji D, Fan Z, et al. Synthesis and 0.88 μm near-infrared electroluminescence properties of a soluble chloroindium phthalocyanine. Dyes and Pigments 2008;76(2):492–8.
[8] Kulkarni AP, Zhu Y, Jenekhe SA. Quinoxaline-containing polyfluorenes: synthesis, photophysics, and stable blue electroluminescence. Macromolecules 2005;38(5):1553–63.
[9] Gunes S, Baran D, Gunbas G, Ozyurt F, Fuchsbauer A, Sariciftci NS, et al. Photovoltaic and photophysical properties of a novel bis-3-hexylthiophene substituted quinoxaline derivative. Solar Energy Materials & Solar Cells 2008;92(9):1162–9.
[10] Thomas KRJ, Velusamy M, Lin JT, Tao Y-T, Chuen C-H. Chromophore-labeled quinoxaline derivatives as efficient electroluminescent materials. Chemistry of Materials 2005;17(7):1860–6.
[11] Yamamoto T, Sugiyama K, Kushida T, Inoue T, Kanbara T. Preparation of new electron-accepting π-conjugated polyquinoxalines. Chemical and electrochemical reduction, electrically conducting properties, and use in light-emitting diodes. Journal of the American Chemical Society 1996;118(16):3930–7.
[12] Cui Y, Zhang X, Jenekhe SA. Thiophene-linked polyphenylquinoxaline: a new electron transport conjugated polymer for electroluminescent devices. Macromolecules 1999;32(11):3824–6.
[13] Burrows HD, Fonseca SM, Gigante B, Esteves MA, Guerreiro AM. Fluorescence study of dehydroabietic acid-based bipolar arylamine–quinoxalines. Journal of Fluorescence 2006;16(2):227–31.
[14] Touzani R, Ben-Hadda T, Elkadiri S, Ramdani A, Maury O, Le Bozec H, et al. Solution, solid state structure and fluorescence studies of 2,3-functionalized quinoxalines: evidence for a π-delocalized keto-enamine form with N–H…O intramolecular hydrogen bonds. New Journal of Chemistry 2001;25:391–5.
[15] Itoh T. Photophysical processes in quinoxaline vapor at low pressure. Spectrochimica Acta Part A: Molecular and Biomolecular Spectroscopy 2003;59(13):3019–27.
[16] Pan Y, Sheng Z, Ye X, Ao Z, Chu G, Dai J, et al. Photochemistry of quinoxaline derivatives and mechanism of the triplet state quenching by electron-poor alkenes. Journal of Photochemistry and Photobiology A: Chemistry 2005;174(2):98–105.
[17] Kishida H, Hirota K, Wakabayashi T, Okamoto H, Lee B-L, Kokubo H, et al. Third-order nonlinear optical spectroscopy in charge-transfer type conjugated polymers. Synthetic Metals 2005;153(1–3):141–4.
[18] Jaung J-Y. Synthesis and halochromism of new quinoxaline fluorescent dyes. Dyes and Pigments 2006;71(3):245–50.
[19] Mac M, Danel A, Wisla A, Karocki A, Krolicki R. Electron transfer and intersystem crossing processes in new dyes based on 1H-pyrazolo[3,4-b]quinoxaline: effect of temperature and solvent polarity on the CT fluorescence. Journal of Photochemistry and Photobiology A: Chemistry 2006;180(1–2):88–100.
[20] Barberis VP, Mikroyannidis JA, Spiliopoulos IK. Synthesis and optical properties of quinoxaline-containing poly(aryl ether)s. Synthetic Metals 2007;157(10–12):475–80.
[21] Kim J-H, Jaung JY. The synthesis and optical properties of meso-substituted porphyrins bearing quinoxaline derivatives. Dyes and Pigments 2008;77(2):474–7.
[22] Jang CK, Jaung J-Y. The synthesis and optical properties of quinoxalines bearing 2,2′:6′,2″-terpyridine. Dyes and Pigments 2009;80(1):168–73.
[23] Arun V, Robinson PP, Manju S, Leeju P, Varsha G, Digna V, et al. A novel fluorescent bisazomethine dye derived from 3-hydroxyquinoxaline-2-carboxaldehyde and 2,3-diaminomaleonitrile. Dyes and Pigments 2009;82(3):268–75.
[24] Blau W. Organic materials for nonlinear optical devices. Physics in Technology 1987;18:250–68.

[25] Arun V, Sridevi N, Robinson PP, Manju S, Yusuff KKM. Ni(II) and Ru(II) Schiff base complexes as catalysts for the reduction of benzene. Journal of Molecular Catalysis A: Chemical 2009;304(1–2):191–8.
[26] Gazit A, App H, McMahon G, Chen J, Levitzki A, Bohmer FD. Tyrphostins. 5. Potent Inhibitors of platelet-derived growth factor receptor tyrosine kinase: structure-activity relationships in quinoxalines, quinolines, and indole tyrphostins. Journal of Medicinal Chemistry 1996;39(11):2170–7.
[27] Mamedov VA, Kalinin AA, Gubaidullin AT, Isaikina OG, Litvinov IA. Synthesis and functionalization of 3-ethylquinoxalin-2(1H)-one. Russ. Journal of Organic Chemistry 2005;41(4):599–606.
[28] Bozdyreva KS, Aliev ZG, Maslivets AN. Five-membered 2,3-dioxo heterocycles: LVII. Recyclization of 3-pivaloylpyrrolo[1,2-a]quinoxaline-1,2,4(5H)-triones by the action of o-phenylenediamine. Crystalline and molecular structure of 3-[3,3-dimethyl-2-oxo-1-(3-oxo-3,4-dihydroquinoxalin-2-yl)butyl]-1-phenylquinoxalin-2(1H)-one. Russian Journal of Organic Chemistry 2008;44(4):607–11.
[29] Kotb ER, Anwar MA, Soliman MS, Salama MA. Synthesis and reactions of some novel quinoxalines for anticancer evaluation. Phosphorus Sulfur Silicon and the Related Elements 2007;182:1119–30.
[30] Cheeseman GWH, Werstiuk ESG. Qninoxaline chemistry. Developments 1963–1975. Advances in Heterocyclic Chemistry 1978;22:367–431.
[31] Selvakumar PM, Suresh E, Subramanian PS. Synthesis, spectral characterization and structural investigation on some 4-aminoantipyrine containing Schiff base Cu(II) complexes and their molecular association. Polyhedron 2007;26(4):749–56.
[32] Ahmed M, Khanl ZH. Electronic absorption spectra of benzoquinone and its hydroxy substituents and effect of solvents on their spectra. Spectrochimica Acta Part A: Molecular and Biomolecular Spectroscopy 2000;56(5):965–81.
[33] Hao Y, Xu B, Gao Z, Wang H, Zhou H, Liu X. Optical properties, electronic energy level structure and electro-luminescent characteristics of salicylaldehyde anil zinc. Journal of Materials Science and Technology 2006;22(2):225–9.
[34] Brown GH, Graham B, Vittum PW, Weissberger A. Azomethine dyes. I. color and constitution of pyrazolone azomethine dyes. Journal of the American Chemical Society 1951;73(3):919–26.
[35] Katritzky AR, Kucharska HZ, Rowe JD. Potentially tautomeric pyridines. Part VI. 2-, 3-, and 4-phenacylpyridines. Journal of the Chemical Society; 1965:3093–6.
[36] Katritzky AR, Ghiviriga I, Oniciu DC, O'Ferrall RAM, Walsh SM. Study of the enol-enaminone tautomerism of α-heterocyclic ketones by deuterium effects on ^{13}C chemical shifts. Journal of the Chemical Society, Perkin Transactions 1997;2:2605–8.
[37] Ledbetter Jr JW. Spectroscopic evidence for the enol imine-keto enamine tautomerism of *N*-(*o*-and *p*-hydroxybenzylidene) anils in solution. Journal of Physical Chemistry 1966;70(7):2245–9.
[38] Nicholson RS, Shain I. Theory of stationary electrode polarography. Single scan and cyclic methods applied to reversible, irreversible, and kinetic systems. Analytical Chemistry 1964;36(4):706–23.
[39] Yanilkin VV, Mamedov VA, Toropchina AV, Kalinin AA, Nastapova NV, Morozov VI, et al. Redox active surface films produced by electrooxidation of substituted indolysines. Russian Journal of Electrochemistry 2006;42(3):212–24.
[40] Isse AA, Abdurahman AM, Vianello E. Self-protonation mechanism in the electroreduction of hydroxyimines. Journal of the Chemical Society, Perkin Transactions 1996;2:597–600.
[41] Isse AA, Gennaro A, Vianello E. Electrochemical reduction of Schiff base ligands H_2salen and H_2salophen. Electrochimica Acta 1997;42(13–14):2065–71.
[42] Tonzola CJ, Alam MM, Kaminsky W, Jenekhe SA. New n-type organic semiconductors: synthesis, single crystal structures, cyclic voltammetry, photophysics, electron transport, and electroluminescence of a series of diphenylanthrazolines. Journal of the American Chemical Society 2003;125(44):13548–58.
[43] Mancilha FS, DaSilveira Neto BA, Lopes AS, Moreira Jr PF, Quina FH, Goncalves RS, et al. Are molecular 5,8-extended-quinoxaline derivatives good chromophores for photoluminescence applications? European Journal of Organic Chemistry 2006;21:4924–33.
[44] Li J, Ma C, Tang J, Lee C-S, Lee S. Novel starburst molecule as a hole injecting and transporting material for organic light-emitting devices. Chemistry of Materials 2005;17(3):615–9.
[45] Sheik-Bahae M, Said AA, Wei T, Hagan DJ, Van Strayland EW. Sensitivitive measurement of optical nonlinearities using a single beam. IEEE Journal of Quantum Electronics 1990;26:760–9.